

Angular Power Distribution of Wireless Channel in Mine Tunnels

Yu Huo^{*1}, Ting-Ting Wang², Feng-Xue Liu³, Zhao Xu⁴

^{1,2,3,4}IOT Perception Mine Research Center, China University of Mining and Technology
Xuzhou, Jiangsu 221008, China, +86 0516 83899705

^{1,2,3,4}School of Information and Electrical Engineering, China University of Mining and Technology

*Corresponding author, e-mail: huoyupaper@yahoo.cn^{*1}; xuzhao551@163.com⁴

Abstract

The statistical characteristics of the angular power distribution of the wireless channel in mine tunnels are the concern of this paper. Firstly, we develop a ray-based channel model which provides the angular power spectrum (APS) in tunnels. We discuss the allowed rays existing in a tunnel based on the modal theory. The number of the allowed rays is limited. The directions of the rays are discrete. They are influenced by the excitation conditions. And then we deduce the propagation parameters as the functions of the direction of arrival (DOA) for each ray to reduce the computational burden. The model is validated by experimental measurements. Then theoretical results deduced from our model show that APS in the tunnel follows Gaussian distribution. For vertical polarization, the spread of the azimuth angle is more sensitive to the excitation conditions. While for horizontal polarization, the spread of the elevation angle is more sensitive.

Keywords: wireless channel, angular power distribution, angle spread, ray-based model, communication in tunnels

Copyright © 2013 Universitas Ahmad Dahlan. All rights reserved.

1. Introduction

In underground mines, wireless communication using natural wave propagation is a low-cost, easy to implement and scalable solution, so it is more flexible and efficient than the wire-based or leaky coaxial cable guided systems. However, due to the rock and coal bounding of the tunnel walls, the propagation characteristics of electromagnetic signals are quite different from the terrestrial wireless channels. The multipath fading in underground tunnels is much more severe. Consequently, bidirectional high-gain antenna, phased antenna, Multiple-Input-Multiple-Output (MIMO), and other the Third Generation (3G) or beyond-3G techniques are studied recently to against multipath fading and improve the radio coverage in these environments [1]-[3]. To achieve the optimal performance of these systems, the spatial characteristics when signal travels in a tunnel must be considered. They are characterized by APS. And the angle spread (AS) deduced by APS reflects the spatial range in which the energy is concentrated [4], [5]. However, the published work concerning the characteristics of multi-path propagation in tunnels mainly focused on the fading distribution and the power delay profile [3,6-8]. Theoretical results of the spatial characteristics of the channel have been obtained to date are very few.

Zhang [6] measured the received signal power versus the width or the height of the tunnel cross section in two tunnels. The curves show distorted cosine function. Lienard [9] measured and calculated the DOA for the successive rays at a distance of 40m in a tunnel. It is shown that the energy is concentrated in a direction corresponding nearly to the tunnel axis. And the angle spread (AS) increases with the tunnel size. This can be due to the phenomena that there are more rays in the larger tunnel. Nasr [10] and Zheng [11] calculated DOA in a rectangular tunnel by the ray method. However, they neglected the effect of the waveguide made by the tunnel itself on the effectively excitation and the propagation of the rays. They supposed that there are myriad rays excited from the transmitting antenna, and that the rays could be transmitted in any direction. We consider that the direction and the number of the possible rays are limited and should vary with the tunnel conditions.

The purpose of this paper is to develop an in-depth analysis on the spatial characteristics of the wireless channel in mine tunnels.

The remainder of this paper is organized as follows. In Section 2, the existing channel model is introduced, and then a ray-based channel model is developed in detail. We discuss which rays and how many rays could be effectively excited in the tunnel in actual. On this basis, the propagation parameters of each ray according to DOA are deduced to simplify the ray tracing process. In Section 3, the expression for APS in tunnels is provided. In Section 4, simulation results are provided. The model is validated by compared with the experimental measurements available in the literature. And then we analyze the statistical characteristics of the angular power distribution of the channel in underground mines. Finally, the paper is concluded in Section 5.

2. Ray-based Channel Model

The angular distribution of the multi-path components can be computed from measurements or simulations.

For measurement campaigns, the accuracy is high, but also the cost in materials and human. Moreover, the results are short of commonality.

For simulations, currently there are mainly two models: waveguide model [12], [13] and ray model [14]-[18].

For the waveguide model [12], [13], the intensity of each mode depends on the excitation, but it cannot be given by this model. This drawback could be avoided by the ray approach, which describes approximately the transmission of each mode by a ray. Nevertheless, although the ray models have been developed for 30 years, most of them neglect the effect of the waveguide made by the tunnel itself on the effectively excitation and the propagation of the rays. They consider that the excitation of the rays in the tunnel is the same as the terrestrial wireless channels [14]-[18]: the transmitter could excite the ray that effectively propagates in a tunnel in any direction, and the number of the rays is myriad. Then the received field in the tunnel is a summation of all geometrically possible rays. However, in the further work of the modal theory we have developed in [12], it is shown that the number of the progressive propagating waves made by the allowed modes in a tunnel is limited and varies with the tunnel excitation conditions, such as the tunnel size and the carrier frequency. Consequently, the approach adopted in the general ray models will cause inaccurate theoretical results of the wireless channel, especially of the angular power distribution in the tunnel.

In this section, we provide a novel ray model. Theoretical analysis of the direction and the number of the allowed rays are developed for tunnel environments. Moreover, the functional relationship between the propagation parameters of each ray and its direction in a tunnel are deduced to simplify the complicated iterative process of the general ray tracing method. These propagation parameters include: the number of reflections, the grazing angles, the length, and the arriving location of the ray when it arrived at the tunnel cross section containing the receiver. The proposed model is validated by both theoretical deduction and experimental results.

2.1. Tunnel Environment

Although the actual tunnel cross sections are generally in-between a rectangle and a circle, the electromagnetic field distribution and attenuation of the modes in the rectangle waveguide are almost the same as the circular waveguide [9], [19]. Besides, to get sufficient wireless coverage in mine tunnels, the tunnels are always divided into elementary cells and let each antenna cover one short section [20]. So we treat the tunnel cross section as an equivalent rectangle as most of the propagation models.

Suppose that the rectangular tunnel walls consist of coal and rock. Consider K_1 and K_2 are the electrical parameters of the material on the vertical walls and the horizontal walls, respectively. The width and height of the tunnel are described by w and h , respectively. The coordinate system is located in the centre of the tunnel cross section. z axis is defined as the longitudinal direction of the tunnel, x axis as the width, and y axis as the height.

2.2. Excitation of Rays

When the wavelength is somewhat smaller than the tunnel dimensions, the tunnel could be considered as a rectangular waveguide. The modes existing in the tunnel are actually all

possible solutions for the Maxwell's equations. Due to the cut-off frequency, the allowed modes number is limited, and it is a variable depending on the propagation conditions [12]. For ray approaches, the ray is used to describe approximately the propagation of each mode [13], [15]. So the progressive propagating waves produced by the rays must reproduce the modes behavior. The angles of departure (AOD) of the allowed rays should be equal to that of the corresponding allowed mode, and the number of the allowed rays should be equal to the number of the transmission modes in the tunnel.

Suppose that the (m, n) mode bounces from wall to wall of the tunnel making a grazing angle ϕ_1 with the side walls and ϕ_2 with the floor and roof. They are given by the following equations [12],

$$\phi_1 \cong \arcsin\left(\frac{m\lambda}{2w}\right); \phi_2 \cong \arcsin\left(\frac{n\lambda}{2h}\right) \tag{1}$$

where $m=0, \pm 1, \pm 2, \dots, \pm m_{\max}$, and $n=0, \pm 1, \dots, \pm n_{\max}$. λ is the wavelength.

Suppose that the angles of (m, n) mode emitted from the source are characterized by its elevation angle θ_D and azimuth angle φ_D . θ_D is the angle of the ray with respect to y axis; φ_D is the angle of the horizontal projection of the ray with respect to x axis. The boundaries of them are $[0, \pi]$ and $[0, 2\pi]$, respectively. Figure 1 shows the angle parameters of a ray in three-dimensional coordinate system. Then we obtain,

$$\begin{aligned} \varphi_D &= \delta\pi + \frac{\pi}{2} \pm \arcsin\left(\frac{\sin \phi_1}{\cos \phi_2}\right) \\ &= \delta\pi + \frac{\pi}{2} \pm \arcsin\left(\frac{m}{w\sqrt{4/\lambda^2 - n^2/h^2}}\right) \end{aligned} ; \theta_D = \frac{\pi}{2} \pm \phi_2 = \frac{\pi}{2} \pm \arcsin\left(\frac{n\lambda}{2h}\right) \tag{2}$$

If the receiver is in the front of the transmitter, $\delta=0$. Otherwise, $\delta=1$.

From (2), the maximum value of allowed m and n are,

$$m_{\max} = \frac{2w}{\lambda}; n_{\max} = \frac{2h}{\lambda} \tag{3}$$

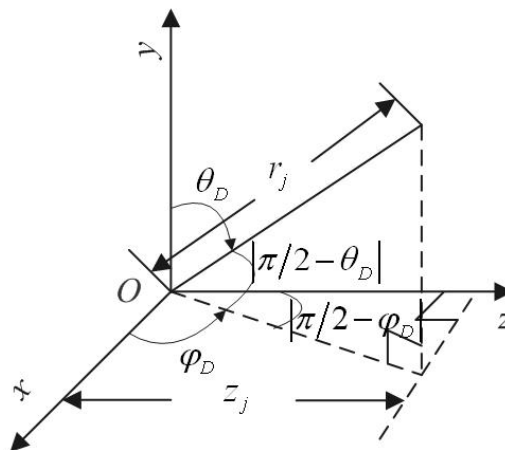


Figure 1. Angle parameters of a ray in three-dimensional coordinate system

If the antenna is bidirectional, the number of the modes M excited in the tunnel is given by

$$\begin{aligned}
M &= 2[(2m_{\max} + 1)(2n_{\max} + 1) - 1] \\
&= \frac{32wh}{\lambda^2} + \frac{8}{\lambda}(w + h)
\end{aligned} \tag{4}$$

According to (2) and (4), the number of the rays which could travel in the tunnel is limited and the AOD for each ray are discrete variables. Moreover, they vary with the propagation conditions, including the wavelength and the tunnel size.

2.3. Geometrical Description of Rays

Once the AOD and the number of the rays are determined, we can trace the propagation of all the excited rays. Nevertheless, the existing tracing methods are complicated iteration algorithm: as soon as a reflection is experience by a ray, the attenuation is calculated, compared and saved in the database. These kinds of approaches cause heavy computational burden, especially in large tunnels.

Here, we provide a method to simplify the complicated calculation of the reflective wave in 3-dimension planes into the calculation in 2-dimension planes. Then the propagation parameters of each ray can be determined directly by its AOD.

To begin with, we give some definitions.

The general case of a ray traveling from S to the cross section containing D in the tunnel is shown in Figure 2. Point S signifies the transmitting antenna, and D the receiving antenna, and D' the point where the ray gets on the receiving cross section. The positions of S, D, and D' are clarified by (x_0, y_0, z_0) , (x, y, z) , and (x', y', z) , respectively. The wave experiences N_1 reflections at the vertical walls and N_2 reflections at the horizontal walls, while traveling a distance r . Direct wave is the special case of reflective waves, for which $N_1=0$ and $N_2=0$.

According to the law of reflection, the incident ray, the normal and the reflected ray lie in the same plane which is called as incident plane. The angle of incidence is equal to the angle of reflection. We draw all the incident planes according to every reflection of the ray SD', as shown in Figure 2. It is shown that the incident planes can be divided into two kinds: the one is perpendicular to the top and bottom of the tunnel, the other is perpendicular to the side walls, then we define them as the 1st kind of incident plane and the 2nd kind of incident plane, respectively.

Secondly, as shown in Figure 3, we project the 1st kind of incident plane on the roof, and get the polygonal line $S_{\parallel}D_{\parallel}'$. The points S_{\parallel} and D_{\parallel}' are clarified by $(x_0, h/2, z_0)$ and $(x', h/2, z)$ respectively. Similarly, project the 2nd kind of incident plane on the right side wall and get the polygonal line $S_{\perp}D_{\perp}'$. The point S_{\perp} is clarified by $(w/2, y_0, z_0)$, and D_{\perp}' by $(w/2, y', z)$. It can be concluded that the number of reflections experienced by the broken lines $S_{\parallel}D_{\parallel}'$ and $S_{\perp}D_{\perp}'$ are equal to N_1 and N_2 respectively.

Suppose that the grazing angles of $S_{\parallel}D_{\parallel}'$ and $S_{\perp}D_{\perp}'$ are ϕ_{\parallel} and ϕ_{\perp} , then we obtain

$$\phi_{\parallel} = \left| \delta\pi + \frac{\pi}{2} - \varphi_D \right|; \quad \phi_{\perp} = \arctan \left| \frac{\cos \theta_D}{\sin \varphi_D \sin \theta_D} \right| \tag{5}$$

Figure 3 shows the 2-dimensional representations of lines $S_{\parallel}D_{\parallel}'$ and $S_{\perp}D_{\perp}'$. Then the computation of N_1 , N_2 , x' and y' of 3-dimension rays are simplified into 2-dimension.

If $0 \leq \varphi_D \leq \pi/2$ or $3\pi/2 \leq \varphi_D \leq 2\pi$,

$$N_1 = \begin{cases} 0 & , |z - z_0| < \frac{\left(\frac{w}{2} - x_0\right)}{\tan \phi_{\parallel}} \\ \left\lceil \frac{|z - z_0| \tan \phi_{\parallel} - w/2 + x_0}{w} \right\rceil + 1 & , |z - z_0| \geq \frac{\left(\frac{w}{2} - x_0\right)}{\tan \phi_{\parallel}} \end{cases} \tag{6}$$

$$x' = (-1)^{N_1-1} \left[N_1 w - (x_0 + |z - z_0| \tan \phi_{\parallel}) \right] \tag{7}$$

If $\pi/2 < \varphi_D < 3\pi/2$,

$$N_1 = \begin{cases} 0 & , |z - z_0| < \frac{\left(\frac{w}{2} + x_0\right)}{\tan \phi_{\parallel}} \\ \left\lfloor \frac{|z - z_0| \tan \phi_{\parallel} - w/2 - x_0}{w} \right\rfloor + 1 & , |z - z_0| \geq \frac{\left(\frac{w}{2} + x_0\right)}{\tan \phi_{\parallel}} \end{cases} \quad (8)$$

$$x' = (-1)^{N_1} [N_1 w + (x_0 - |z - z_0| \tan \phi_{\parallel})] \quad (9)$$

If $0 \leq \theta_D \leq \pi/2$,

$$N_2 = \begin{cases} 0 & , |z - z_0| < \frac{\left(\frac{h}{2} - y_0\right)}{\tan \phi_{\perp}} \\ \left\lfloor \frac{|z - z_0| \tan \phi_{\perp} - h/2 + y_0}{h} \right\rfloor + 1 & , |z - z_0| \geq \frac{\left(\frac{h}{2} - y_0\right)}{\tan \phi_{\perp}} \end{cases} \quad (10)$$

$$y' = (-1)^{N_2-1} [N_2 h - (y_0 + |z - z_0| \tan \phi_{\perp})] \quad (11)$$

If $\pi/2 < \theta_D \leq \pi$,

$$N_2 = \begin{cases} 0 & , |z - z_0| < \frac{\left(\frac{h}{2} + y_0\right)}{\tan \phi_{\perp}} \\ \left\lfloor \frac{|z - z_0| \tan \phi_{\perp} - h/2 - y_0}{h} \right\rfloor + 1 & , |z - z_0| \geq \frac{\left(\frac{h}{2} + y_0\right)}{\tan \phi_{\perp}} \end{cases} \quad (12)$$

$$y' = (-1)^{N_2} [N_2 h + (y_0 - |z - z_0| \tan \phi_{\perp})] \quad (13)$$

To get the distance r of the ray, we divide the ray into $(N_1 + N_2 + 1)$ -segment straight lines. Here we only discuss the general case which the source and the receiver do not belong to the same vertical plane, namely $z \neq z_0$. For every segment, the absolute value of the angle between its projection on horizontal plane and z axis is always $|\delta\pi + \pi/2 - \varphi_D|$, and the absolute value of the angle between it and its projection on the horizontal plane is always $|\pi/2 - \theta_D|$. Figure 1 shows the j th straight line segment with length r_j . The length of the segment projected on z axis is z_j . Then r_j is given by

$$r_j = \frac{z_j}{|\sin \varphi_D| |\sin \theta_D|} \quad (14)$$

Then the total length of the ray from S to D' is

$$r = \sum_j r_j = \frac{\sum_j z_j}{|\sin \varphi_D| |\sin \theta_D|} = \frac{|z - z_0|}{|\sin \varphi_D| |\sin \theta_D|} \tag{15}$$

From (1) and (2), the grazing angles of each ray can also be obtained by the ray's AOD,

$$\phi_1 = \arcsin(|\cos \varphi_D| |\sin \theta_D|); \phi_2 = |\pi/2 - \theta_D| \tag{16}$$

The direction of the ray arriving at the cross section containing the receiver is also characterized by its elevation angle θ and azimuth angle φ . θ is the angle between the arrival and y axis; φ is the angle between the arrival and x axis. Then the AOA for each ray could be obtained as follows,

$$\varphi = \begin{cases} \pi + \varphi_D, & \text{if } N_1 \text{ is even number} \\ 2\pi - \varphi_D, & \text{if } N_1 \text{ is odd number} \end{cases}; \theta = \begin{cases} \pi - \theta_D, & \text{if } N_2 \text{ is even number} \\ \theta_D, & \text{if } N_2 \text{ is odd number} \end{cases} \tag{17}$$

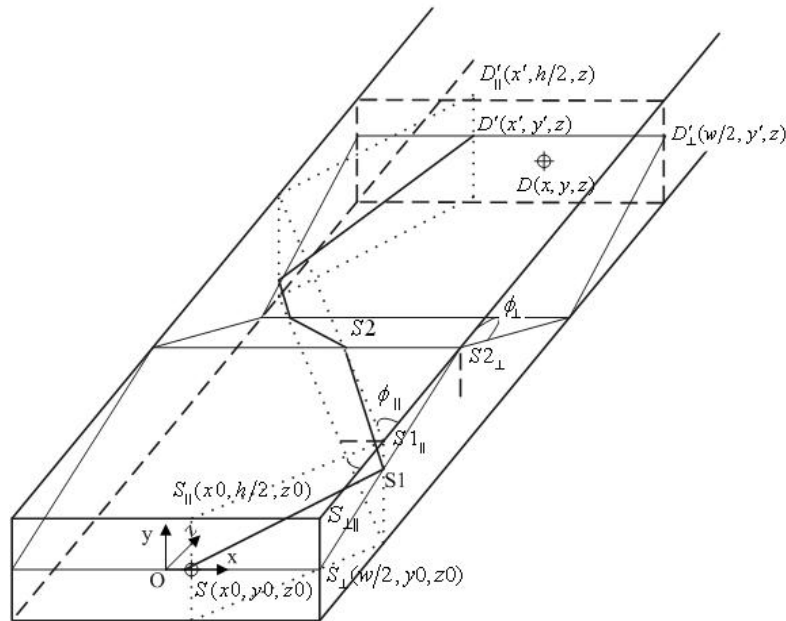


Figure 2. The general case of a ray propagating in a tunnel

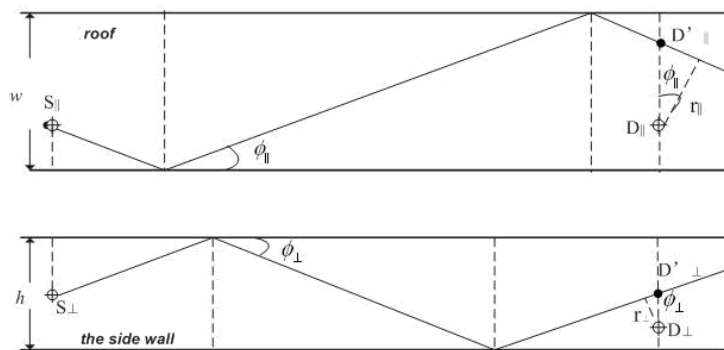


Figure 3. Projection of a 3-dimensional ray on the tunnel walls

2.4. Reception of Rays

When the AOA and the arriving position of the ray are determined, we could calculate the distance between the ray and the receiving antenna. Then whether the allowed ray reaches to the receiver could be decided by a reception sphere [21]. Suppose that the centre of the sphere is the receiving antenna, and the radius is r_0 . If the distance between the ray and the receiving antenna is smaller than r_0 , the ray is effectively received.

3. Angular Power Spectrum

Owing to the multiple reflections, diffractions and diffusions on the tunnel walls, the waves reach to the receiver in different directions, and then the AOD of the signal is expanded. This dispersion effect of the tunnel waveguide will cause the space selective fading of the signal. The angular power distribution could be characterized by the APS. The AS deduced by APS could reflect the range in which the energy is concentrated in the angle domain [4], [5].

At a certain time t , certain emitted angles θ and φ , and position (x,y,z) in the tunnel, the impulse response of the wireless channel is,

$$h(t, \theta, \varphi) = \sum_{i=1}^M a_i \exp(-j2\pi f \tau_i) \delta_{ri} \delta[t - \tau_i] \delta[\theta - \theta_i] \delta[\varphi - \varphi_i] \quad (18)$$

where τ_i is the delay of the i th ray,

$$\tau_i = \frac{r_i}{c} = \frac{|z - z_0|}{c |\sin \varphi_D| |\sin \theta_D|} \quad (19)$$

$$\delta_{ri} = \begin{cases} 1 & \text{if the } i\text{th ray reaches to the receiver} \\ 0 & \text{if the } i\text{th ray does not reach to the receiver} \end{cases} \quad (20)$$

a_i is the field strength of the i th ray. It should be normalized to the overall transmitting power.

Combined with the ray model [15], the field strength of the i th ray is the function of the reflections number, the grazing angles and the length of the ray discussed in (5)-(16). The dis-normalized field strength of the i th is,

$$A_i = \frac{\lambda}{4\pi} \frac{\sqrt{G_i R_1^{(i)} R_2^{(i)}}}{r_i} \quad (21)$$

in which, G_i is the antenna gains of the i th ray. R_1 and R_2 are the Fresnel reflectance from the side walls/the roof and floor. Then R_1 and R_2 are given by the following formulas.

For horizontally polarized rays,

$$R_1^{(h)} = \left| \frac{K_1 \sin |\phi_1| - (\sin^2 |\phi_1| + K_1 - 1)^{1/2}}{K_1 \sin |\phi_1| + (\sin^2 |\phi_1| + K_1 - 1)^{1/2}} \right|^{N_1}; \quad R_2^{(h)} = \left| \frac{\sin |\phi_2| - (\sin^2 |\phi_2| + K_2 - 1)^{1/2}}{\sin |\phi_2| + (\sin^2 |\phi_2| + K_2 - 1)^{1/2}} \right|^{N_2} \quad (22)$$

For vertically polarized rays,

$$R_1^{(v)} = \left| \frac{\sin |\phi_1| - (\sin^2 |\phi_1| + K_1 - 1)^{1/2}}{\sin |\phi_1| + (\sin^2 |\phi_1| + K_1 - 1)^{1/2}} \right|^{N_1}; \quad R_2^{(v)} = \left| \frac{K_2 \sin |\phi_2| - (\sin^2 |\phi_2| + K_2 - 1)^{1/2}}{K_2 \sin |\phi_2| + (\sin^2 |\phi_2| + K_2 - 1)^{1/2}} \right|^{N_2} \quad (23)$$

Then a_i is,

$$a_i = \sqrt{|A_i|^2 / \sum_{i=1}^M |A_i|^2} \quad (24)$$

For a signal $s(t, \theta, \varphi)$ travels in the channel, the received power in the direction of (θ, φ) is

$$P(\theta, \varphi) = \left| \sum_{i=1}^M a_i \exp(-j2\pi f \tau_i) \delta_{\theta, \varphi} s(\theta - \theta_i, \varphi - \varphi_i) \right|^2 \quad (25)$$

Define θ_0 , φ_0 as the mean path AOA. σ_θ , σ_φ as the AS, which are the root-mean-square of arrived angles,

$$\theta_0 = E\{\theta\}; \quad \varphi_0 = E\{\varphi\} \quad (26)$$

$$\sigma_\theta = \sqrt{E\{\theta^2\} - [E\{\theta\}]^2}; \quad \sigma_\varphi = \sqrt{E\{\varphi^2\} - [E\{\varphi\}]^2} \quad (27)$$

in which $E[\cdot]$ is the mathematical expectation function.

4. Results and Analysis

4.1. Comparison with Experimental Measurements and General Ray Approaches

4.1.1. Electric-field Intensity with Different Axial Distance

(1) Comparison with Experimental Measurements

To validate the ray model, we firstly compare our theoretically predicted field intensity with the experimental measurements in a tunnel environment provided in [22, Figure 18].

In [22, Figure 18], the experiments were conducted in a tunnel. It is an equivalent rectangular tunnel of 3.5 km length, 5.3 m height, and 7.8 m width. The transmitting and receiving antennas were at the same height (2 m). Both antennas were placed at horizontal positions of one-quarter of the tunnel width. They focused on the vertical polarization at the frequencies of 450 MHz and 900 MHz. At 450 MHz, half-wave vertical dipoles were used, while at 900 MHz, vertically polarized wide-band horn antennas were used, the gain of which is 7dBi. Using the same parameters stated above, we calculate the electric-field intensity in dBm by our proposed ray model that considers the effects of the waveguide made by the tunnel itself on the excitation of the rays in Figure 4(a). The curves of the theoretical results and the experimental results in [22, Figure 18] are close to each other. It is shown that the field intensity is stronger for 900 MHz than 450MHz. The reason is that the smaller the wavelength is compared with the tunnel size, the freer the waves propagate, and then there are more modes contributing to the propagation.

(2) Comparison with General Ray Approaches

To compare and validate that our model is more rationality than the general ray models, we also calculated the electric-field intensity without considering the waveguide effects of the tunnel on the excitation of the rays as [14]- [18] in Figure 4(b). The results show that there is different tendency between the curves in Figure 4(b) and Figure 18 in [22]. The field intensity is stronger for 450MHz than 900 MHz. If the excitation of the rays is not restricted by the waveguide effects, the parameters such as the reflections number, the grazing angles and the length of each ray traveling from the transmitter and the receiver in a tunnel are constant no matter which frequency is, as soon as the locations of the antennas are determined. And the number of the rays is myriad. Under theses conditions, the field intensity of each ray varies inversely with the carrier frequency according to (21). Then the overall received field as the summation of all possible rays becomes weaker for higher frequency. Consequently, the waveguide effects on the excitation of the rays can not be neglected.

4.1.2. AOA of the Rays in a Tunnel

(1) Comparison with Experimental Measurements

In [9, Figure 4(b)], the spread of the AOA of the rays determined from the complex impulse response was measured in a rectangular tunnel that is 5 m wide, 6 m high. The average value of the electrical parameters of the tunnel walls is $5-j0.01$. The transmitter and the receiver adopted half-wave vertical dipoles. They were 40m apart. The signal has a centre frequency of 450MHz. Using the same parameters, we calculate the map of the DOA by our ray model in Figure 5. As the same as [9, Figure 4(b)], the AOA of the successive rays is depicted as a function of the excess time delay normalized to the first received pulse and the amplitude of the signal expressed in decibels. In the map, the ordinate is the excess time delay, and the abscissa is the cosine of the angle A between the tunnel axis and the ray, while the signal amplitude is given by the color scale. By comparison, our proposed ray-based channel model is validated to the experimental results.

(2) Comparison with General Ray Approaches

Another simulation utilizing the general ray model without considering the tunnel waveguide effects has been made in [9, Figure 4(a)]. By comparison with these maps, the result produced by our ray model and the experimental result are closer to each other. While the result produced by the general ray model in [9, Figure 4 (a)] shows that the spread of the AOA of the successive rays are much wider than our theoretical and the experimental results. Because it considers more directions in which the rays actually can not be effectively excited in the tunnel.

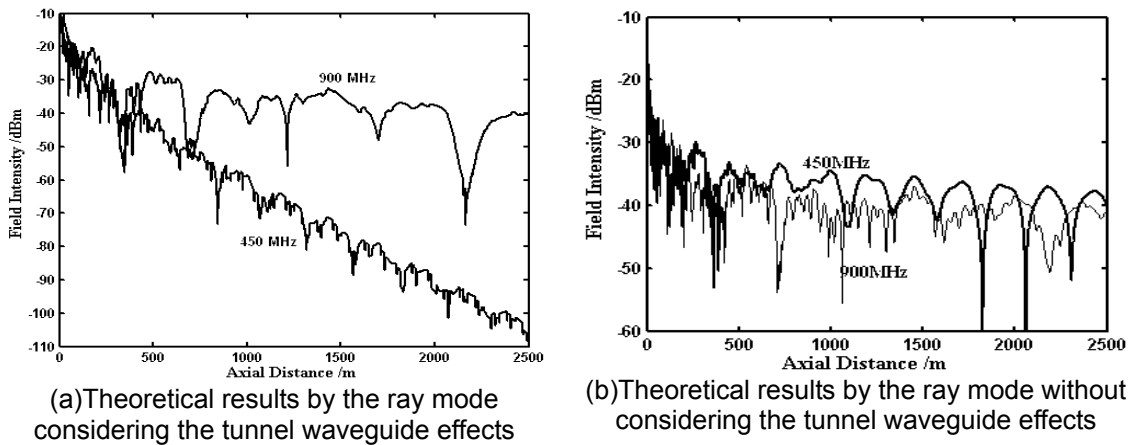


Figure 4. Electric-field intensity as a function of the axial distance

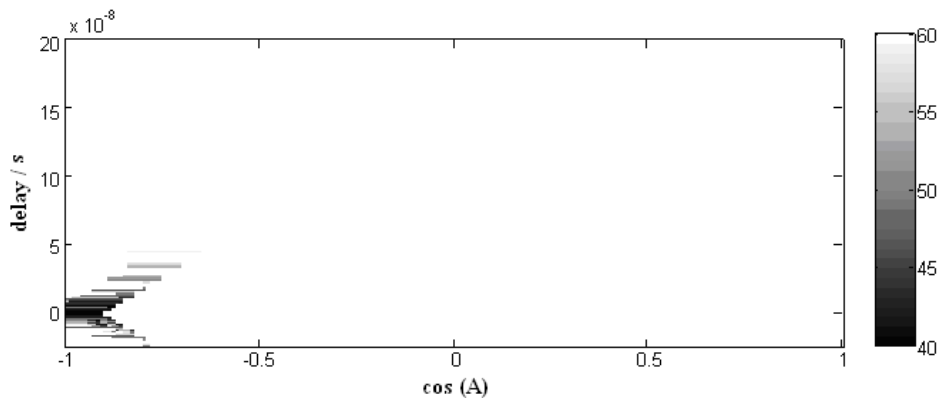


Figure 5. DOA of the rays represented in the plane ($\cos(A)$ -delay)

4.2. Angular power distribution in a rectangular tunnel

APS is decided by the tunnel size, carrier frequency, antenna positions, and so on. In this section, we begin with an initial example that illustrates the AOA distribution in a rectangular tunnel. Then we analyze the influence of the above parameters on it respectively.

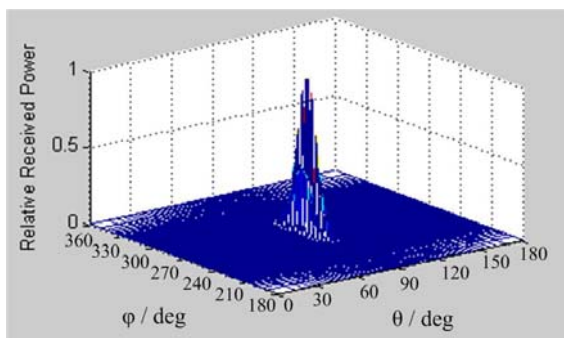
Except studying the effects of certain parameters, the default tunnel conditions are set as follows: the tunnel cross section shape is a rectangle with a width of 7.8 m and a height of 5.3 m; consider the general case that the coal is on all the walls of the tunnel and $K_1=K_2=10-j0.18$; the carrier frequency is set to 900 MHz; the transmitter/receiver is vertically polarized isotropic antenna and located centrally, and the axial distance between them $|z-z_0|$ is 100 m.

4.2.1. Initial example

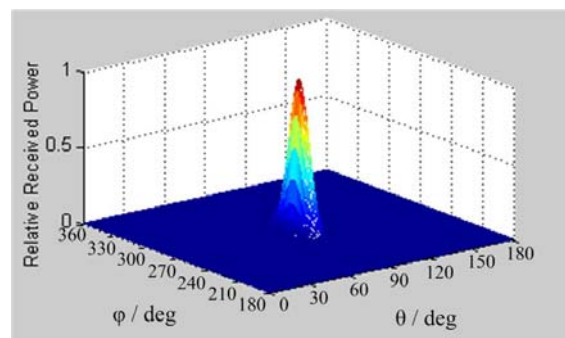
Figure 6(a) presents APS deduced from our ray model in the above environment. To compare, APS is normalized to the pulse with strongest power.

Different probability density functions (PDFs) for the angular distribution of the incident waves have been proposed in the literature [23], such as \cos^n distribution, Gaussian distribution and Laplacian distribution. For \cos^n distribution, there is a close relationship between the angle spread and the sign “ n ”. For the small AOA spread computed in Figure 6(a), n is on the order of 100. In this case, the curve for the \cos^n PDF is extremely close to the Gaussian PDF.

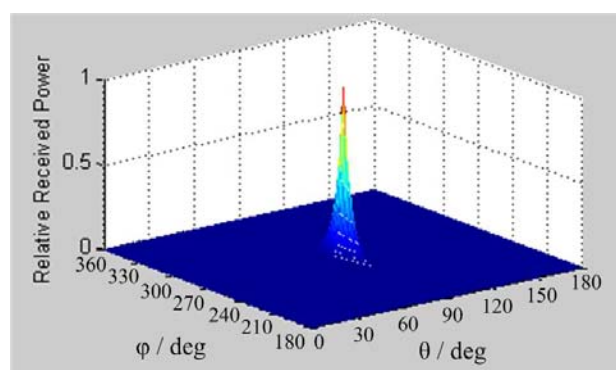
Here we compute the probability distribution corresponding to the Gaussian law in Figure 6(b) and to the Laplacian law in Figure 6(c), respectively. To generate graphs of the probability density function, the values of them have been calculated so that θ_0 , φ_0 , σ_θ and σ_φ deduced either from the Gaussian/Laplacian distribution or from the actual distribution of the field are identical.



(a) Distribution deduced from theoretical values



(b) Gaussian distribution



(c) Laplacian distribution

Figure 6. Angular power spectrum of arrival in a rectangular tunnel

By comparison, we get a good agreement between the figures in Figure 6(a) and (b), whereas there is a significant difference between the figures in Figure 6(a) and (c). So it can be concluded that AOA distribution in the rectangular tunnel follows Gaussian distribution.

Zheng [11] considered that the directions of the rays are successive and uniform, so the calculated results of APS shows the Laplacian distribution. The difference between the conclusions shows that the waveguide effect is rather significant when model the wireless channel in tunnels once again.

4.2.2. Influence of Different Excitation Conditions

1) Influence of tunnel size

From (1), (2) and (17), φ is mostly relevant to the width of the rectangular tunnel, and θ is mostly relevant to the height of the rectangular tunnel. So by simulations, we could find that the tunnel width plays little role in σ_θ and the tunnel height plays little role in σ_φ . Here we mainly analyze the influence of width on σ_φ and the height on σ_θ .

In Figure 7 we compute σ_φ with a range of the width in the tunnel of a fixed height, 5.3 m. We also calculate σ_θ with a range of the height in the tunnel of a fixed width, 5.3 m.

We note that the variations of σ_φ and σ_θ are fluctuating. This is due to the fact that from (2), the angles of departure of the limited excited rays are discrete variables that do not vary continuously with the tunnel size. Attributed to the similar reason, this phenomenon also exists in the following simulations in terms of the influences of the carrier frequency and antenna position.

Besides, it is clear that the larger the tunnel size, the larger the mean value of σ_φ and σ_θ in Figure 7. Because the larger the tunnel dimension is, the freer the waves propagate, which causes that the tunnel is closer to free-space environment.

We also note that the percentage increase of the mean σ_φ is much larger than that of the mean σ_θ . The reason is that the reflection coefficients on the vertical walls are much larger than those on the horizontal walls for vertically polarized waves. Consequently, there are less rays received in the vertical planes of the antenna, the spread of the elevation angle θ is so small that its variation is not significant. All in all, the spread of the azimuth angle φ is more sensitive to the excitation conditions, and the tunnel width plays a more important role.

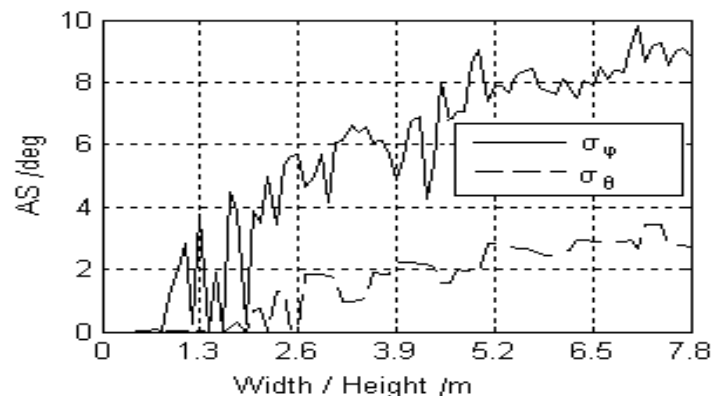


Figure 7. σ_φ versus width of the tunnel of 5.3 m height, and σ_θ versus height of the tunnel of 5.3 m width

2) Influence of carrier frequency

We illustrate the effects of operating frequency on σ_θ and σ_φ in Figure 8. The curves show that the mean angular spread varies directly with the frequency when the frequency is

lower than 500 MHz. This is because that: 1) there are only a few rays for lower frequency, and most of them has very large grazing angles which causes great attenuation; 2) the number of the rays increases with the increasing frequency according to the previous discussion. While when the frequency is higher than 500 MHz, weak descendent tendency occurs, especially for σ_ϕ . This could be explained by that: 1) there are multiple significant rays for these frequencies; 2) the grazing angles of each ray become smaller, and then more and more significant rays concentrated in the direction of the tunnel axis for the signal with higher operating frequency, which causes the decrease in AS. But when the frequency is higher than 1200MHz, the variation of σ_θ and σ_ϕ becomes gradual. This is because that, there are so many rays for these frequencies that the spatial densities of the rays are similar to each other, which causes that the mean AS closes to a constant for these higher frequencies. The occurrence frequency of weak decrease in the AS and gradual variation of the AS depends on the tunnel size, the communication distance, and so on.

In Figure 8, it can also be found that the spread of elevation angle θ varies little for different frequencies. The reason is consistent with the previous analysis about that the variation of σ_θ is not significant for vertically polarized waves.

3) Influence of antenna

The antenna could affect the spatial distribution of the received power by its position, polarization.

For antenna positions, we fix the transmitting antenna in the center of the tunnel, and conduct the study on two cases: move the receiving antenna along the longitudinal direction of the tunnel; move the receiving antenna along the transverse direction, and the longitudinal distance relative to the transmitter $|z-z_0|$ is unchanged. For the first case, as shown in Figure 9, with the increasing propagation distance $|z-z_0|$, the AS decreases. Since the paths with large grazing angles attenuate very rapidly, the AS decreases fast when near the transmitter. But at great distance from the transmitter, significant rays tend to become parallel to the tunnel axis, so the fall in the AS is gradual. In the second case, we find that the position of the receiver in the transverse section of the tunnel changes AS little ($\sigma_\phi \approx 9.5^\circ$, $\sigma_\theta \approx 2.8^\circ$). That can be explained by the symmetrical geometry shape of the tunnel.

All the above study is performed on the vertical polarization. Because of the symmetrical tunnel shape, the above conclusions of σ_ϕ and σ_θ are exchanged with each other when the antenna is horizontally polarized. σ_θ is more sensitive to the excitation conditions than σ_ϕ . Moreover, the tunnel height affects AS more than the tunnel width.

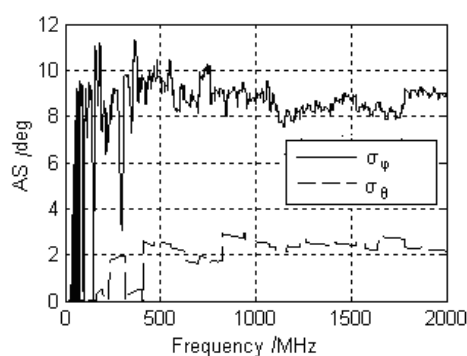


Figure 8. AS versus carrier frequency

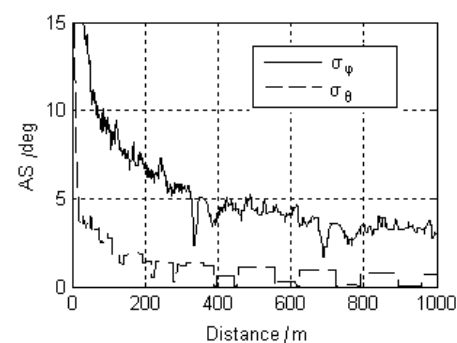


Figure 9. AS versus the axial distance

5. Conclusion

The spatial distribution of the power of the wireless channel in mine tunnels is the concern of this paper. Firstly, we develop a ray-based channel model which provides the APS in a tunnel. We discuss the allowed rays existing in the tunnel on the basis of modal theory. The number of the allowed rays is limited. The direction of the rays is discrete variable. They are

influenced by different excitation conditions. And then we deduce the functional relationship between the propagation parameters and the DOA for each ray to simplify the ray tracing calculation. The ray model is validated by the published experimental measurements. Then based on the proposed channel model, our analysis shows that:

- 1) The APS in the rectangular tunnel follows Gaussian distribution.
- 2) The variation of the AS with the frequency can be divided into three bands. The AS increases rapidly when the frequency is low. A weak fall in the AS occurs when the frequency is high. The variation is gradual when the frequency is higher. The division of these three frequency bands depends on the tunnel size and the communication distance, and so on.
- 3) The antenna position in the cross section of the tunnel changes the AS little.
- 4) For vertical polarization, the spread of the azimuth angle is more sensitive to the excitation conditions than the spread of the elevation angle. The tunnel width affects AS more than the tunnel height.

While for horizontally polarized waves, the spread of the elevation angle is more sensitive, and the tunnel height affects AS more than the tunnel width.

Acknowledgement

This paper is supported by the Special Fund for High-quality Articles of CUMT (No.2012LWB75).

References

- [1] Liu LS, Zhang ZJ, Tian ZJ, and Feng ZH. A Bidirectional Endfire Array with Compact Antenna Elements for Coal Mine/tunnel Communication. *IEEE Antennas and Wireless Propagation Letters*. 2012; 11: 342-345.
- [2] Coraiola A., Sturani B. Using a Pair of Phased Antenna to Improve UHF Reception/Transmission in Tunnel. *IEEE Antennas Propag. Mag.* 2000; 42(5): 40-47.
- [3] Cocheril Y, Combeau P, Berbineau M, and Pousset Y. *MIMO Propagation Channel Characteristics in Tunnels*. Proceedings of the 7th International Conference on Telecommunications (ITST). Sophia Antipolis. 2007: 1-6.
- [4] Zhang LW. Sparsity-based Angle of Arrival Estimation for Emitter Localization. *TELKOMNIKA*. 2012; 10(4): 769-774.
- [5] GUO LM, Nian XH. Time of Arrival and Angle of Arrival Statistics for Distant Circular Scattering Model. *TELKOMNIKA*. 2012; 10(3): 564-571.
- [6] Zhang YP, Hwang Y. Characterization of UHF Radio Propagation Channels in Tunnel Environments for Microcellular and Personal Communications. *IEEE Trans. Veh. Technol.* 1998; 47(1): 283-296.
- [7] Lienard M, Degauque P. Propagation in Wide Tunnels at 2GHz: A Statistical Analysis. *IEEE Trans. Veh. Technol.* 1998; 47(1): 283-296.
- [8] Djadel M, Despins C, and Affes S. *Narrowband Propagation Characteristics at 2.45 and 18GHz in Underground Mining Environments*. Proceedings of Global Telecommunications Conference (GLOBECOM). Taipei. 2002; 2: 1870-1874.
- [9] Lienard M, Degauque P. Natural Wave Propagation in Mine Environments. *IEEE Trans. Antenna Propag.* 2000; 48(9): 1326-1339.
- [10] Nasr A, Molina JM, Lienard M, and Degauque P. *Optimisation of Antenna Arrays for Communication in Tunnels*. Proceedings of the 3rd International Symposium on Wireless Communication Systems (ISWCS). Valencia. 2006: 522-524.
- [11] Zheng HD. Study on the Theory of Radio Propagation and the Key Technologies of MIMO Model in Mine Tunnel. PhD Thesis. Xuzhou: China University of Mining and Technology; 2010.
- [12] Huo Y, Xu Z, Zheng HD. Characteristics of Multimode Propagation in Rectangular tunnels. *Chinese Journal of Radio Science*. 2010; 25(6): 1225-1230.
- [13] Emslie AG, Lagace RL, and Strong PF. Theory of the propagation of UHF radio waves in coal mine tunnels. *IEEE Trans. Antenna Propag.* 1975; AP-23(2): 192-205.
- [14] Chen SH, Jeng SK. SBR image approach for radio wave propagation in tunnels with and without traffic. *IEEE Trans. Veh. Technol.* 1996; 45(3): 570-578.
- [15] Mahmoud SF, Wait JR. Geometrical Optical Approach for Electromagnetic Wave Propagation in Rectangular Mine Tunnels. *Radio Sci.* 1974; 9(12): 1147-1158.
- [16] Zhang YP, Hong HJ. Ray-Optical Modeling of Simulcast Radio Propagation Channels in Tunnels. *IEEE Trans. Veh. Technol.* 2004; 53(6): 1800-1808.
- [17] Zhang S. Tent law and modeling of radio digital communication channel in tunnel. *Journal on Communications*. 2002; 23(11):41-50.

- [18] Zhang HQ, Yu HZ, WANG P, Gao XJ. Multipath transmission modeling and simulating of electromagnetic wave in rectangle tunnel. *Chinese Journal of Radio Science*. 2008; 1(23): 195-200.
- [19] Molina-Garcia-Pardo JM, Lienard M, Nasr A, and Degauque P. On the Possibility of Interpreting Field variations and Polarization in Arched Tunnels Using a Model for Propagation in Rectangular or Circular Tunnels. *IEEE Trans. Antenna Propag.* 2008; 56(4): 1206-1211.
- [20] Liu XL, Zhang YP, and Ng LS. *Design and Implementation of a Novel Network for Underground Wireless Communications*. Proceedings of 2nd International Symposium on Communication Systems, Networks and Digital Signal. Bournemouth. 2000: 88-90.
- [21] Seidl SY, Rappaort TS. Site-specific Propagation Prediction for Wireless In-building Personal Communication System Design. *IEEE Transactions on Vehicular Technology*. 1994; 43(4): 879-891.
- [22] Dudley DG, Lienard M, Mahmoud SF, and Degauque P. Wireless Propagation in Tunnels. *IEEE Antenna Propag. Mag.* 2007; 49(2): 11-26.
- [23] WANG CX. *Modeling MIMO Fading Channels: Background, Comparison and Some Progress*. Proceedings of 2006 International Conference on Communications, Circuits and Systems (ICCCAS). Guilin. 2006: 664-669.